An experimental investigation of oblique entry pressure losses in automotive catalytic converters

Quadri, S. , Benjamin, S.F. and Roberts. C.A.

Original citation & hyperlink:
Quadri, S. , Benjamin, S.F. and Roberts. C.A. (2009) An experimental investigation of oblique entry pressure losses in automotive catalytic converters. Proceedings of the Institution of Mechanical Engineers, Part C: Journal of Mechanical Engineering Science, volume 223 (11): 2561-2569.
http://dx.doi.org/10.1243/09544062JMES1565

Experimental investigation of oblique entry pressure losses in automotive catalytic converters

S. S. Quadri, S. F. Benjamin and C. A. Roberts

Automotive Engineering Applied Research Group, Faculty of Engineering and Computing, Coventry University, Coventry CV1 5FB U.K.

E-Mail:s.benjamin@coventry.ac.uk

Abstract

This study investigates oblique entry pressure loss in automotive catalyst monoliths. Experiments have been performed on a specially designed flow rig using different lengths of monolith (17-100mm) over a range of Reynolds number and angles of incidence (0-75 degrees). Losses were found to be a function of Reynolds number and angle of incidence and a general correlation has been derived. CFD predictions of the flow distribution across axisymmetric catalyst assemblies have been performed. Incorporating the oblique entry loss provided much better agreement with experimental data with the assumption that such losses were constant above an angle of incidence of 81 degrees.

Keywords: Oblique entry; Catalyst: CFD: Flow Maldistribution; Monolith; Pressure loss.

1 Introduction

For reduced emissions and optimum conversion efficiency a uniform flow distribution is required across automotive catalysts. Indeed, the degree of flow uniformity is often used to assess the acceptability of design concepts. Increasingly computational fluid dynamics (CFD) is being used to provide this information. It is therefore essential that flow predictions can be made reliably with acceptable accuracy. Examples of CFD applied to automotive catalysts can be seen in the studies conducted by Lai et al., **[1]**, Kim et al., **[2]** and Benjamin et al., **[3]**, amongst many others. Space constraints on the vehicle often necessitate the use of wide-angled diffusers when connecting the exhaust pipe to the front face of the catalyst. This results in flow separation at the diffuser inlet and flow maldistribution in the monolith. Figure 1 shows a typical exhaust catalyst assembly featuring two monoliths located downstream of a wide angled diffuser along with a representation of the flow field within the diffuser. The monolith itself consists of thousands of channels of small hydraulic diameter (~1mm). Simulating the flow within each of these channels is clearly impractical and so an alternative and widely popular approach has been to model the monolith by treating it as an equivalent continuum or porous medium with a prescribed flow resistance. The channel Reynolds number is such that the flow is laminar within the monolith and with typical monolith lengths of ~100mm a common practice is to assume that its resistance can be described by the Hagen-Poiseuille (H-P) relationship for one-dimensional fully developed flow.

Previous studies by Benjamin et al., **[3-5]** have shown that using the porous medium approach and the H-P relationship under-predicts flow maldistribution. This was explained by the fact that over

much of the front face of the monolith the flow enters the channels obliquely resulting in an extra pressure loss which needs to be accounted for when prescribing monolith resistance. Figure 1 illustrates flow separating at the inlet to the diffuser resulting in the formation of large recirculating regions. A central jet is formed across the diffuser which spreads out near the front face of the monolith and impinges obliquely on the channels away from the centre-line. Incorporating a theoretical expression, derived by Küchemann and Weber **[6]** for oblique entry losses in heat exchangers, resulted in improved CFD predictions for flow maldistribution in axisymmetric and close-coupled systems, **[4, 5]**. However discrepancies between predictions and measurements were still evident and experimental verification for the theoretical formulation was considered necessary.

The behaviour of flow obliquely entering a monolith channel is illustrated schematically in figure 2. The flow approaches the channel with velocity $U_{1,}$ at an angle of incidence, α, and separates at the channel entrance forming a recirculation bubble. Further downstream the flow reattaches becoming fully developed with a mean channel velocity $U_c = (U_2/\varepsilon)$. With reference to figure 2 a non-dimensional oblique pressure loss can be defined as

$$K_{Obl} = \frac{P_{Obl}}{\frac{1}{2}\rho U_1^2} \tag{1}$$

This definition is different to that used by Küchemann and Weber **[6]** who normalised pressure loss using the dynamic head based on U_2 in figure 2. These losses have been studied by a number of researchers, mostly in relation to heat exchangers. Küchemann and Weber **[6]** considered oblique flow incident on a cooler block. They proposed two different formulations. In the first approach it was assumed that the loss was equal to the transverse dynamic head, $\frac{1}{2}\rho V^2$ resulting in

$$K_{Obl} = \sin^2 \alpha \tag{2}$$

The second, more conservative approach was based on an assumption that oblique entry losses occurred only above a certain angle of incidence. This assumption is applicable to heat exchangers featuring low loss entry devices and so would not be applicable to the majority of automotive monoliths.

Moore et al. **[7]** developed a theoretical model applicable to heat exchangers which resulted in equation (3). Their model assumed that the pressure across the channel entrance was uniform and equal to that upstream, so that

$$K_{Obl}=(1-\cos\alpha)^2 \quad (3)$$

This expression was also considered by Mohandes et al., **[8]** and Meyer et al., **[9]** for describing losses in a range of heat exchanger devices.

Persoons et al., **[10]** have recently reported oblique flow losses derived from a rig which presented swirling flow at the front of automotive monoliths. Relatively low incidence angles, up to 33 degrees, were studied for four monolith lengths ($4.3 \leq L/d_h \leq 44$). Their losses were approximately half of those deduced by Küchemann and Weber **[6]** namely

$$K_{Obl} = 0.459 \sin^2 \alpha \quad (4)$$

The present study describes an experiment designed to quantify the oblique entry pressure loss in automotive catalyst monoliths over a wide range of incident angles and monolith lengths for a range of *Re*. These losses were then incorporated into a CFD code and predictions of flow maldistribution within axisymmetric catalyst assemblies were compared with measurements.

2 Measuring oblique flow loss

Figure 3 shows a part of the isothermal test rig used to quantify oblique flow loss. The rig is supplied with compressed air from two large receivers. The flow rate was obtained using a calibrated viscous flow meter. A plenum incorporating a flow straightener is positioned upstream of a contracting nozzle which provides uniform flow to an automotive catalyst monolith placed at various angles, α.

The overall pressure loss across the monolith is due to:

- Fully developed laminar flow in the channel
- Boundary layer development in the channel entrance region
- Contraction and expansion losses at the entry and exit of monolith channels
- Oblique entry flow losses due to flow separation at the channel entrance.

The fully developed flow inside a channel resulting from viscous shear at the walls is given by the H-P formulation.

$$\frac{\Delta P_m}{L} = -2f\, Re_c \frac{\mu U_c}{dh^2} \quad (5)$$

Shah's correlation **[11]** accounts for the developing boundary layer and is given by

$$\frac{\Delta P_d}{\frac{1}{2}\rho U_c^2} = (f_{app}\, Re_c)(4X^+) = (f\, Re_c)(4X^+) + K(X) \tag{6}$$

where *K(X)* is zero at the channel entrance and increases to a constant value *K(∞)* when the flow is fully developed.

The contraction and expansion losses at the inlet and exit of the monolith channels are due to abrupt changes in cross-sectional area. A study by Wendland et al., **[12]** showed that the contribution of these losses was around 5% of the total pressure loss for a 400 cpsi monolith.

Hence, with reference to figure 3 the total pressure loss across the system is given by

$$P_{t1} - P_{t2} - P_L - P_{Obl} = 0 \tag{7}$$

with

$$P_{t1} = P_{s1} + \frac{1}{2}\rho\alpha_1 U_1{}^2 \tag{8}$$

$$P_{t2} = P_{s2} + \frac{1}{2}\rho\alpha_2 U_2{}^2 \tag{9}$$

where P_s is the static pressure, U_i the average velocity and α_i the kinetic energy correction factor. Assuming the flow to be one-dimensional (see sections 3.1 & 3.2), α_1 and α_2 are unity. P_L corresponds to the total loss when the incidence angle, α, is zero.

There are also pressure losses in the pipe upstream of the monolith, between station 1 and the front face of the monolith. As the incidence angle increases the length of the upstream pipe also increases. This results in an additional pressure loss which varies with α. This is implicitly accounted for when measuring the pressure differential P_{s1}- P_{s2} and is small.

Hence, equation 7 can be rewritten and normalised to give

$$K_{Obl} = \frac{P_{Obl}}{\frac{1}{2}\rho U_1{}^2} = \frac{(P_{s1} - P_{s2}) + \frac{1}{2}\rho(U_1{}^2 - U_2{}^2) - P_L}{\frac{1}{2}\rho U_1{}^2} \tag{10}$$

3 Methodology

Unwashcoated ceramic monoliths of lengths 17 mm, 27 mm, 40 mm and 100 mm were used from one supplier, and a 69 mm length monolith from another. All featured channels of square cross-section with a nominal cell density of 400 cpsi, hydraulic diameter of 1.12 mm and a porosity of 0.77. The incident angle was varied by placing ducts at different angles (0^0, 30^0, 45^0, 55^0, 60^0, 70^0, 75^0) upstream of the monolith as shown in figure 3.

3.1 Calibration of the rig

The test rig was calibrated by removing the monolith and placing an outlet sleeve 20 mm in length at the nozzle exit. The velocity profiles downstream of the nozzle along x (horizontal) and y (vertical) axes were measured using a TSI IFA 300 constant temperature HWA system at different mass flow rates. The probes used were 5µm platinum plated tungsten wire (Dantec 55 P11) and were calibrated using a fully automatic TSI 1129 calibration rig. The velocity profiles in figure 4 show that the flow is approximately uniform along both axes.

3.2 Hot-wire velocity profiles at the exit of oblique angled ducts

One of the implicit assumptions is that the flow field approaching the monolith is uniform. The intersection of the upstream pipe and the monolith was elliptical when α was greater than 0^0 with the major axis increasing with α . Velocity profiles along the major axis are shown in figure 5. These cases were the worst conditions for flow uniformity. The profiles obtained were, however, considered to be acceptably uniform.

3.3 Static pressure measurements

The differential static pressure measured between points 1 and 2 in figure 3 were obtained using a FC 016 Furness Controls digital manometer with a pressure range of 0-199.9 mm of water (0-1960 Pa) and an accuracy of ± 1 digit or ± 1% of the reading whichever is greater. The velocity downstream of the monolith U_2 was obtained from conservation of mass. To evaluate P_L, measurements were performed at zero degree angle of incidence.

4 Experimental results

4.1 Measurement at zero incidence

The experiments for zero incidence were performed for all monoliths and a range of Reynolds number. The variations in static pressure measurements were less than 2%. The results were plotted as P_L against velocity and an example is shown in figure 6a where a best fit second order polynomial has been fitted to the data. The non-dimensional pressure is compared with the H-P and Shah correlation in figure 6b for all monoliths. It can be seen that the Shah's correlation fits the data well for X^+ greater than 0.02 and the H-P relationship is seen to be a good fit for X^+ greater than 0.2. The findings are similar to a previous study, **[3]**.

4.2 Measurements at incidence

Experiments were performed for 30^0, 45^0, 55^0, 60^0, 70^0 and 75^0 angles of incidence, for all monolith lengths and for a range of Reynolds number ($200 \leq Re_a \leq 2200$). The pressure loss attributable to the monolith P_L was obtained using the polynomial equations obtained from the zero degree angle of incidence measurements and K_{Obl} was obtained from equation 10. As the incidence angle increases, the cross-sectional area of the monolith on which the flow is incident also increases. Hence, for the same mass flow rate, the channel velocity and the pressure loss across the monolith reduce as the angle of incidence increases.

An error analysis was performed by Quadri **[13]** based on the terms of equation 10 and it was found that the errors induced in K_{Obl} are mainly due to errors in U_1 and U_2 and P_L, which in turn is dependent on U_2. The contribution of static pressure measurement errors (P_{s1}-P_{s2}) was much smaller. The measurement uncertainties at low angles of incidence are high due to the fact that K_{Obl} is obtained from the difference of two relatively large numbers (P_{s1}-P_{s2}) and P_L as seen in equation 10. As the angle of incidence increases the channel velocity decreases and the magnitude of P_L is smaller. Hence errors are reduced at high incidence and were around ±5% for 75^0 angle of attack at Re_a=2200 for all lengths. For short monoliths, the magnitude of P_L is smaller and uncertainties are reduced. Excluded from the analysis are data where the derived oblique losses were calculated to be negative or where the measurement uncertainties were estimated to be greater than 100%. This excluded data mainly for cases with low *Re* and/or low angles of incidence.

Figure 7 shows K_{Obl} against $\sin^2 \alpha$, the theoretical expression deduced by Küchemann and Weber **[6]**. For each angle values of K_{Obl} are shown for monoliths of different lengths and various Re_a. For any particular angle the spread is large due in part to the experimental error but also because K_{Obl} increases with Re_a as shown in figure 8. Although there was some indication that K_{Obl} was dependent on monolith length the evidence was inconclusive. Also shown on figure 7 are the theoretical relationships, equations (3) and (4), deduced by Moore & Torrence **[7]** and Persoons et al. **[10]** respectively. The expression by Moore et al underestimates the losses at low angles. The expression by Persoons et al, was derived from data where the maximum incidence was 33^o and it is not possible to deduce its validity here because uncertainties at low incidence are very large. Certainly at higher incidence their expression is not generally applicable but that of Moore et al tends towards the Küchemann and Weber formulation and the observations of this study at high values of α.

5 NON-DIMENSIONAL ANALYSIS

Non dimensional analysis suggests a relationship should exist between K_{Obl} and independent dimensionless groups of the form

$$K_{Obl} = f[\mathrm{Re}_a, \sin^2 \alpha] \tag{11}$$

A relationship of the form given in equation (12) was examined and values of *A* and *n(α)* deduced as below.

$$K_{Obl} = A\mathrm{Re}_a^{\,n(\alpha)} \sin^2 \alpha \tag{12}$$

where

	A	*n(α)*
$30^o \leq \alpha \leq 45^o$,	0.021	0.5
$55^o \leq \alpha \leq 70^o$,	0.18 .	0.24
$\alpha = 75^o$	0.525	0.1

Figure 9 shows an improved correlation when compared with figure 7.

6 AXISYMMETRIC CFD STUDY

Equation 12 was assessed by incorporating the oblique entry loss in CFD simulations using STAR-CD V 3.26 software **[14]** on an axisymmetric model and comparing predictions with experimental results obtained in an earlier study **[4]**. In that study a conical diffuser of 60^0 total angle was placed upstream of a monolith. The flow maldistribution across the monolith was obtained from HWA measurements at the rear of the monolith. CFD simulations were performed using the Küchemann Weber (K-W) expression, equation (2), for oblique pressure loss. The CFD model of Benjamin et al., **[4]** formed the basis of the present simulation. The V2F turbulence model **[15]** was used in this study and a mesh modification was made so that there were 20 cells in the near wall region to ensure a y^+ value of < 1 was obtained.

The monolith losses were simulated by adding the oblique entry pressure loss from equation (12) to the H-P relationship. The latter was used as it is a good approximation for the monolith and velocity range of this study. Simulations were performed for two flow rates and two monolith lengths. Using the H-P relationship without the oblique entry pressure loss always under-predicts the flow maldistribution (figure 10 b-e). Incorporating equation (12) improved velocities in the central region of the monolith (figure 10a) but the predictions were too low in the region of 10-30 mm from the wall. In this region the flow is at high incidence to the monolith channels and the oblique entry pressure loss is very high relative to H-P resistance. As a consequence the flow is forced towards the wall subsequently increasing predicted channel velocities in the near wall region.

In an attempt to improve predictions of the minimum channel velocities the effect of restricting the oblique entry pressure losses was investigated. It was therefore assumed that above a critical angle of incidence, α_c, the oblique losses remained constant. This implies that the separation bubble at the channel entrance, as shown in figure 2, has a maximum size. This seems a reasonable assumption as clearly the channel height will impose a restriction on the degree of flow separation.

Figure 10a shows that with $\alpha_{c,}$ of 81 degrees good agreement was achieved. Applying this to the other cases shown in figures 10 b-e also provided good agreement with measurements. Also shown on these figures are predictions using the K-W expression along with a critical angle of 81 degrees. There is a small difference, only noticeable on the axis, when predictions are compared to those made using equation 12 with $\alpha_{c,}$ = 81 degrees. Both expressions predict similar values of oblique pressure losses for this range of Re_a. The sensitivity of the minimum velocities to α_c may be explained as follows. If it is assumed that there is no critical angle of incidence then the pressure drop along the channel at the point of minimum velocity, where the angle of incidence is α, is given by

$$P_{s1} - P_{s2} = P_L + P_{Obl} \tag{13}$$

For small channel velocities P_L is approximately directly proportional to U_2 as shown in figure 6a and oblique flow losses are given by

$$P_{Obl} = \frac{1}{2}\rho V^2 = \frac{1}{2}\rho U_2^2 \tan^2 \alpha \tag{14}$$

Hence

$$P_{s1} - P_{s2} = kU_2 L + \frac{1}{2}\rho U_2^2 \tan^2 \alpha \tag{15}$$

where k is a constant. So for $\alpha > \alpha_c$ oblique pressure losses are reduced according to equation (16)

$$P_{Obl} = \frac{1}{2}\rho U_2^2 \tan^2 \alpha_c \text{ where } \alpha_c < \alpha \tag{16}$$

Assuming the same pressure loss, P_{s1}-P_{s2}, U_2 will therefore increase to a value given by the solution of equation (15) with α replaced by α_c. By way of example figure (11) shows the variation of the minimum axial velocity immediately upstream of the monolith as a function of α_c for the test case shown in figure 10a. Figure 11 shows that without imposing a critical angle, the minimum velocity was 1.5 m/s at an angle of incidence 86 degree. With α_c =81 degrees the minimum velocity was increased to 2.52 m/s which is in close agreement with the calculated velocity of 2.8 m/s using the solution of equation (15). This resulted in the minimum velocity downstream of the

monolith, U_2, increasing from 1.75 to 2.64 m/s as shown in figure 10a in close agreement with measurements.

7 CONCLUSION

An experimental study has been performed to measure the oblique entry loss for flow entering catalyst monolith channels. Experiments were performed on an oblique angle flow rig using different lengths of monolith (17mm $\leq L \leq$ 100 mm) over a range of Reynolds number ($200 \leq Re_a \leq 2200$) at different angles of incidence ($0^0 \leq \alpha \leq 75^0$).

The results show that as the angle of incidence increases, the oblique entry loss increases. It was also found to be dependent on the Reynolds number. The rate of increase with Reynolds number was found to be dependent on the angle of incidence. The results were compared with expressions from previous studies. It was found that the K-W expression does not fit the data well. The expression of Persoons et al.**[10]** was not applicable for high angle of incidence and that of Moore et al. **[7]** underestimated the losses at low angles. An improved correlation for oblique entry pressure losses dependent on Reynolds number and angle of incidence was obtained.

The correlation for oblique entry pressure was incorporated into CFD predictions for an axi-symmetric system. It was found necessary to limit the oblique entry loss above a critical angle of 81 degrees to provide better agreement with experimental data at regions of the monolith where the angle of incidence was greater than this. Hence an improved methodology to predict flow distribution in axisymmetric catalyst systems has been obtained.

REFERENCES

1. **Lai, M. C., Kim, J. Y., Cheng, C. Y., Li, P., Chu, G.** and **Pakko, J. D.** Three-dimensional simulations of automotive catalytic converter internal flow. SAE Paper 910200, 1991

2. **Kim, J. Y., Lai, M. C., Li, P.** and **Chu, G.** Modeling diffuser-monolith flows and its implications to automotive catalyst converter design. SAE Paper 921093, 1992

3. **Benjamin, S. F., Clarkson, R. J., Haimad, N.** and **Girgis, N. S.** An experimental and predictive study of flow in axisymmetric automotive exhaust catalyst systems. *SAE Trans., J. Fuels and Lubricants*, 1996 **105**, Sec. 4, 1008-1019

4. **Benjamin, S. F., Haimad, N., Roberts, C. A.,** and **Wollin, J.** Modelling the flow distribution through automotive catalytic converters. *Proc. Inst. Mech. Engrs , Part C:J. Mechanical Engineering Science*, 2001, **215** (C4), 379-383

5. **Benjamin, S. F., Zhao, H., Arias-Garcia, A.** Predicting the flow field inside a close-coupled catalyst-the effect of entrance losses. *Proc. Inst. Mech. Engrs, Part C:J. Mechanical Engineering Science*, 2002, **217** (C4), 283-288

6. **Küchemann, D.** and **Weber, J**. *Aerodynamics of propulsion*, 1953 (McGraw-Hill, New York).

7. **Moore, F. K.** and **Torrence, K. E.** Air flow in dry natural-drought cooling towers subject to wind. Cornell Energy multiple-tube systems, Cornell Energy Report, Ithaca, New York, 1977.

8. **Mohandes M. A., Jones T. V.** and **Russell, C. M. B.** Pressure loss mechanisms in resistances inclined to an air flow with application to fin tubes. First National Heat Transfer Conference, Leeds, 1984.

9. **Meyer C. J.** and **Kroger D. G.** Air-cooled heat exchanger inlet flow losses. *Applied Thermal Engineering*, 2001, **21** (7), 771-786.

10. **Persoons, T., Vanierschot, M.** and **Van den Bulck, E.** Oblique inlet pressure loss for swirling flow entering a catalyst substrate, *Exp. Therm. Fluid Sci*., 2008, **32**, 1223-1231

11. **Shah, R. K.** A correlation for laminar hydrodynamic entry length solutions for circular and noncircular ducts. *Transactions of the ASME, Journal of Fluids Engineering*, 1978, **100**, 177-179.

12. **Wendland, D. W., Sorell, P. L.** and **Kreucher, J. E.** Sources of monolith catalytic converter pressure loss. SAE Paper 912372, 1991.

13. **Quadri, S. S.** The effect of oblique entry flow in automotive catalytic converters. Ph.D. thesis, Coventry University, U.K, 2008

14. *STAR-CD Manual version 3.26,* 2004 (Computational Dynamics).

15. **Iaccarino, G.** Predictions of a turbulent separated flow using commercial CFD codes. *Transactions of the ASME, Journal of Fluids Engineering*, 2001 **123**, 819-828

APPENDIX

NOTATION

A	coefficient in equation 12
C_μ	constant of turbulence
d_h	channel hydraulic diameter, m
f	friction Fanning factor for fully developed flow, dimensionless
f_{app}	apparent friction Fanning factor, dimensionless
k	permeability coefficient in equation 15 ($kg/m^3.s$)
$K(X)$	additional pressure loss term for developing flow, dimensionless
$K(\infty)$	additional pressure loss term for developed flow, dimensionless
K_{Obl}	non-dimensional oblique entrance pressure loss, $(P_{Obl} / \frac{1}{2}\rho U_1^2)$
$K_{Obl,\ Expt.}$	experimental non-dimensional oblique entrance pressure loss
$K_{Obl,\ Pred.}$	predicted non-dimensional oblique entrance pressure loss
L	monolith length, m
n	exponent in equation 12
P_s	static pressure, Pa
P_t	total pressure, Pa
P_L	pressure loss at zero incidence, Pa
ΔP_m	pressure loss due to fully developed flow across the monolith, Pa
ΔP_d	pressure loss due to developing flow at the entrance of the channels + pressure loss due to fully developed flow, Pa
P_{Obl}	oblique entrance pressure loss, Pa
Re	Reynolds number based on upstream inlet pipe diameter, dimensionless
Re_a	approach Reynolds number, $(\rho U_1 d_h / \varepsilon\mu)$
Re_c	channel Reynolds number, $(\rho U_c d_h / \mu)$
U_1	upstream velocity in the oblique angled ducts, m/s

U_2	outlet velocity downstream of the substrate, m/s , ($U_1 \cos\alpha$)
U_c	channel velocity, m/s, ($U_1 \cos\alpha / \varepsilon$)
V	transverse velocity component upstream of the monolith, m/s ($U_1 \sin\alpha$)
X	distance along channel, m
X^+	dimensionless monolith length, ($X / d_h . Re_c$)
y	distance from the wall, m
y^+	normalized distance from the wall, ($\rho C_\mu \kappa^{1/2} . y / \mu$)

Greek Symbols

α	angle of incidence (^{o})
α_c	critical angle of incidence (^{o})
α_1	kinetic energy correction factors for inlet velocity U_1, dimensionless
α_2	kinetic energy correction factors for exit velocity U_2, dimensionless
ε	porosity of the monolith, dimensionless
κ	turbulent kinetic energy, m^2/s^2
ρ	density of air, kg/m^3
μ	dynamic viscosity of the fluid, Pa.s

Abbreviations

CFD	computational fluid dynamics
cpsi	cells per square inch
HWA	hot-wire anemometry
H-P	Hagen-Poiseuille relationship
K-W	Küchemann and Weber

List of figure captions

Fig 1 Schematic diagram showing catalyst configuration comprising of two monoliths in an exhaust system, catalyst channels and flow separation in a diffuser.

Fig 2 Schematic diagram showing oblique flow entering catalyst channels with the formation of a recirculation bubble at the channel entrance

Fig 3 Schematic diagram of the flow rig

Fig 4 Nozzle velocity profiles along the *x* and *y* axes

Fig 5 Hot-wire velocity profiles at exit from 27 mm monolith for different angles of incidence.

Fig 6a Monolith pressure drop for 100 mm monolith

Fig 6b Non-dimensional monolith pressure loss $(P_{s1}-P_{s2})/ (^1/_2\rho U_c^2)$ compared with H-P, equation (5), and Shah, equation (6).

Fig 7 Comparison of K_{Obl} against the theoretical assumption of $\mathrm{Sin}^2\alpha$

Fig 8 K_{Obl} dependence on approach Reynolds number (Re_a) for 27 mm monolith

Fig 9 Comparison of experimental and predicted K_{Obl} using equation (12)

Fig 10 Comparison between experimental data (symbols) and CFD predictions (line curves). (a) 152 mm monolith; *Re* 79900. CFD: equ. (12) with/without α_c (b) 152 mm monolith; *Re* 79900. CFD: K-W and equ. (12) both with α_c and H-P (no oblique losses). (c) 152 mm monolith; *Re* 58300. CFD: as (b). (d) 102 mm monolith; *Re* 35900. CFD: as (b). (e) 102 mm monolith; *Re* 83200. CFD: as (b).

Fig 11 Minimum axial velocities immediately upstream of the 152 mm monolith at *Re* 79900

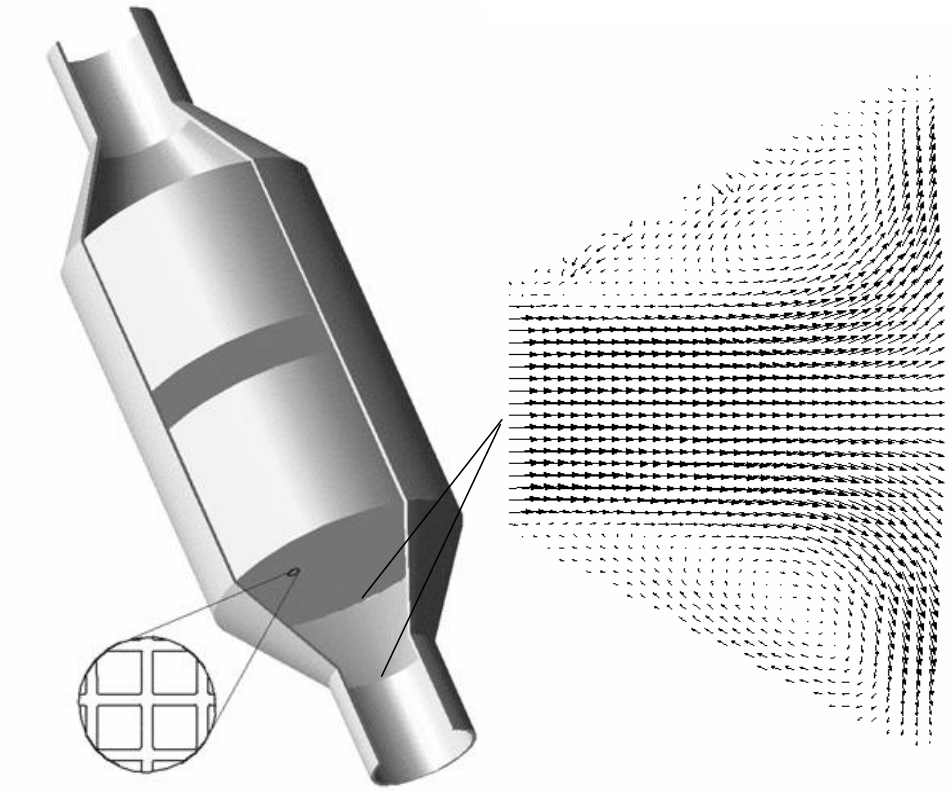

Fig 1 Schematic diagram showing catalyst configuration comprising of two monoliths in an exhaust system, catalyst channels and flow separation in a diffuser

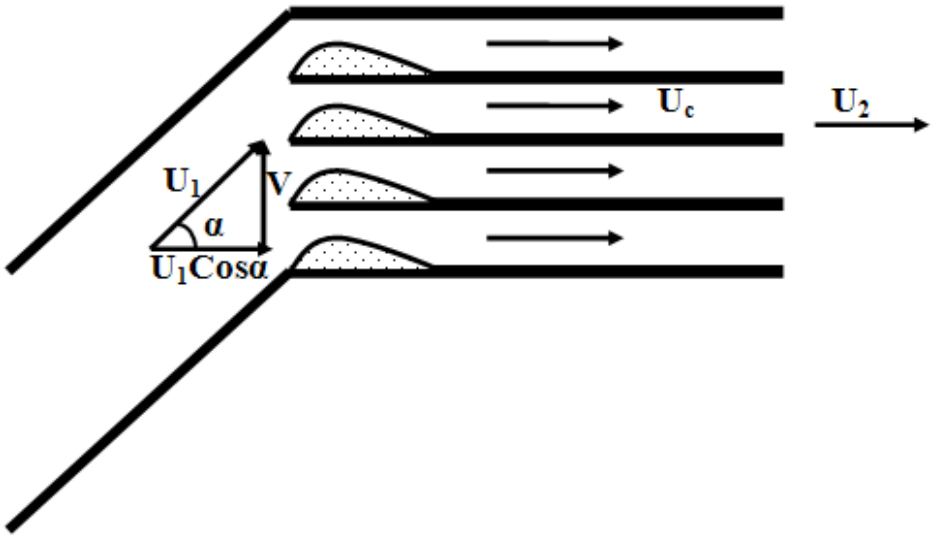

Fig 2 Schematic diagram showing oblique flow entering catalyst channels with the formation of a recirculation bubble at the channel entrance

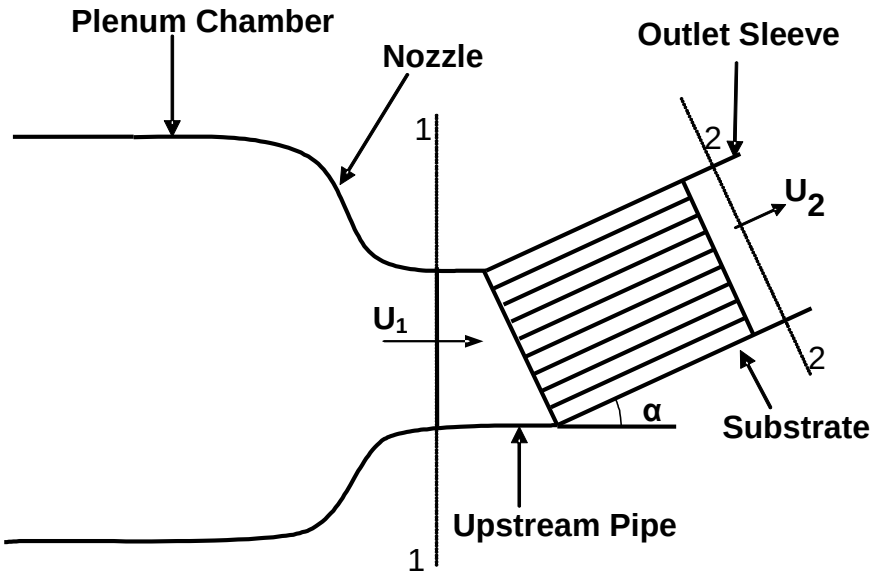

Fig 3 Schematic diagram of the flow rig

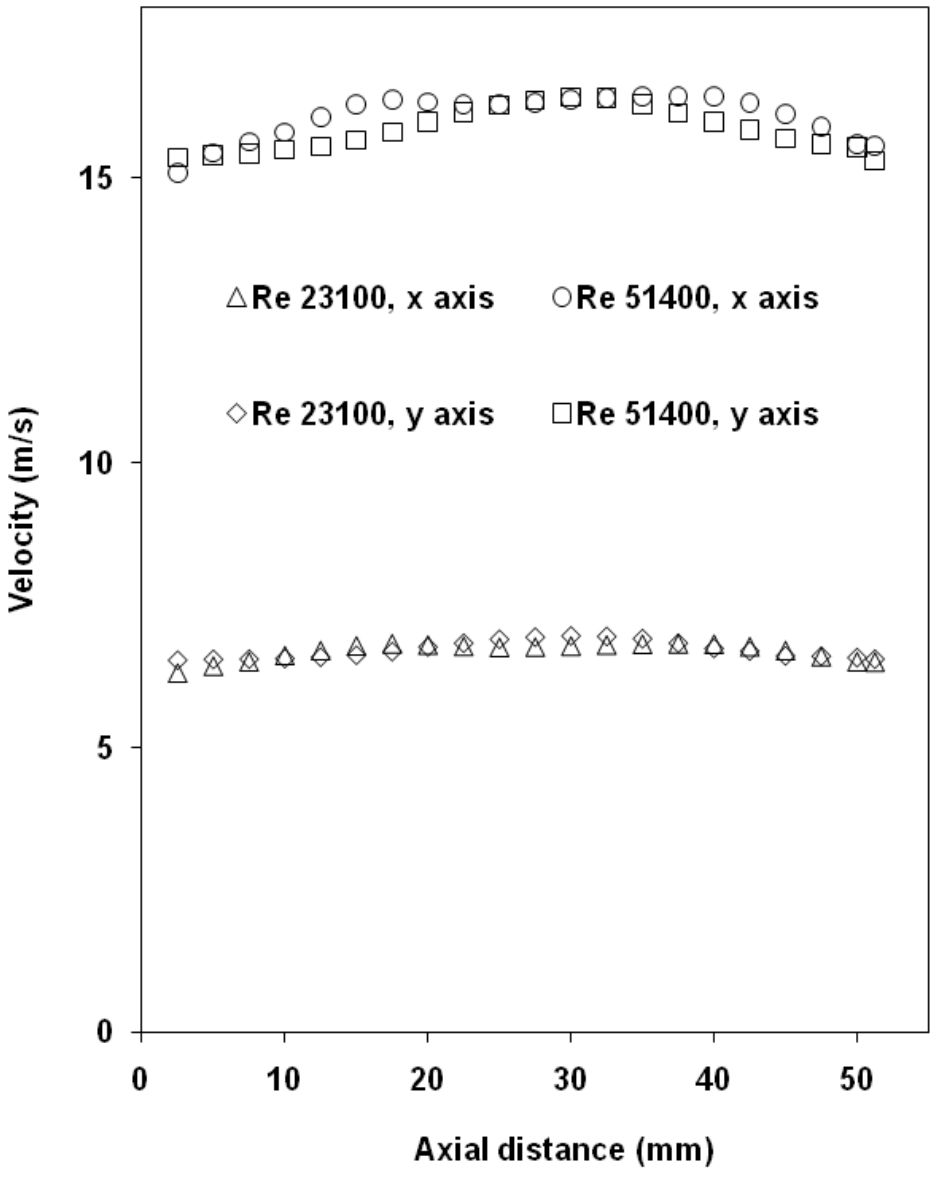

Fig 4 Nozzle velocity profiles along the x and y axes

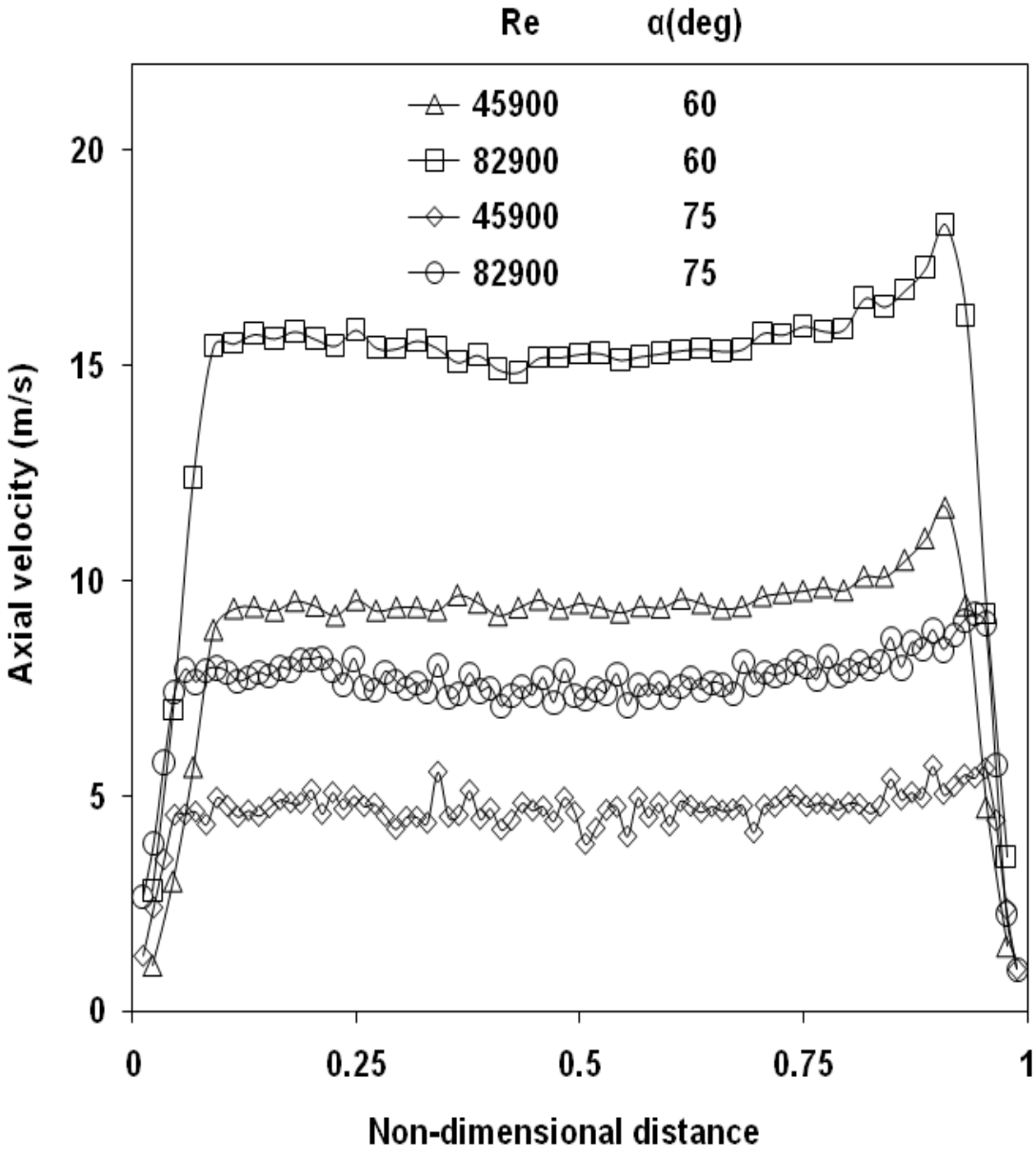

Fig 5 Hot-wire velocity profiles at exit from 27 mm monolith for different angles of incidence.

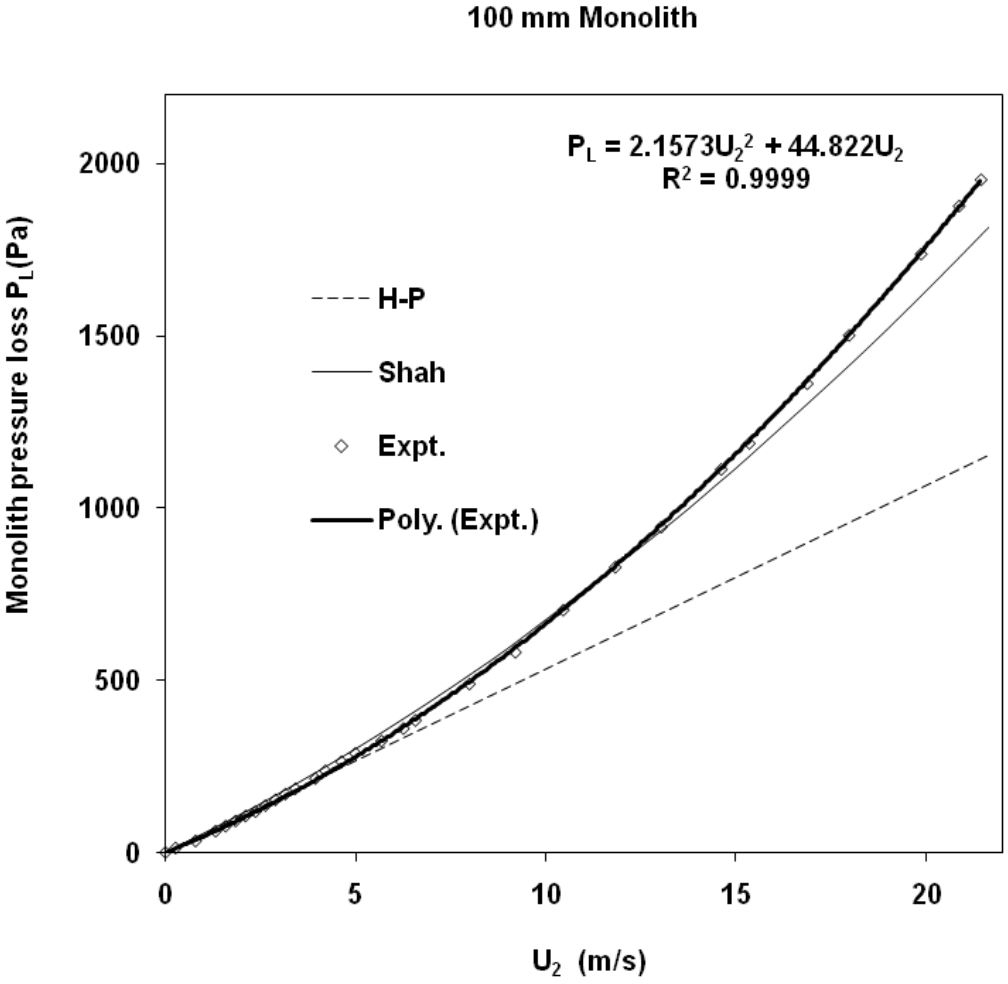

Fig 6-a Monolith pressure drop for 100 mm monolith

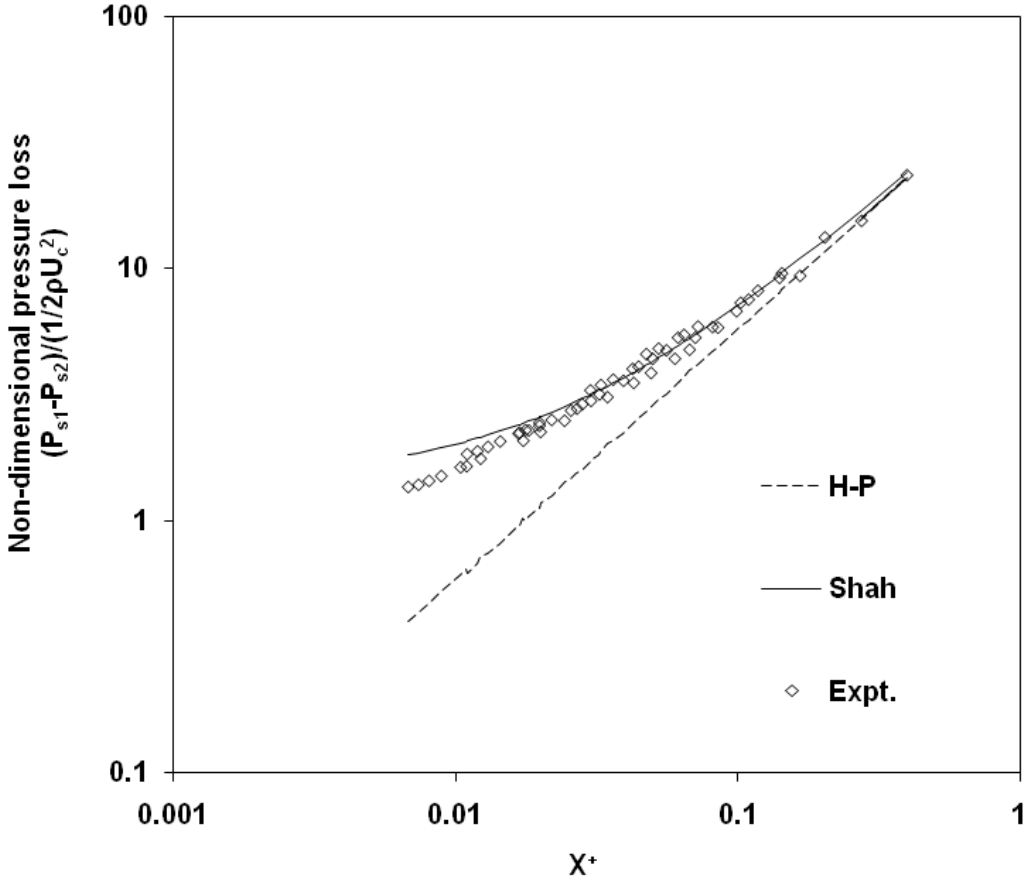

Fig 6-b Non-dimensional monolith pressure loss (P_{s1}-P_{s2})/ ($^1/_2\rho U_c^2$) compared with H-P, equation (5), and Shah, equation (6).

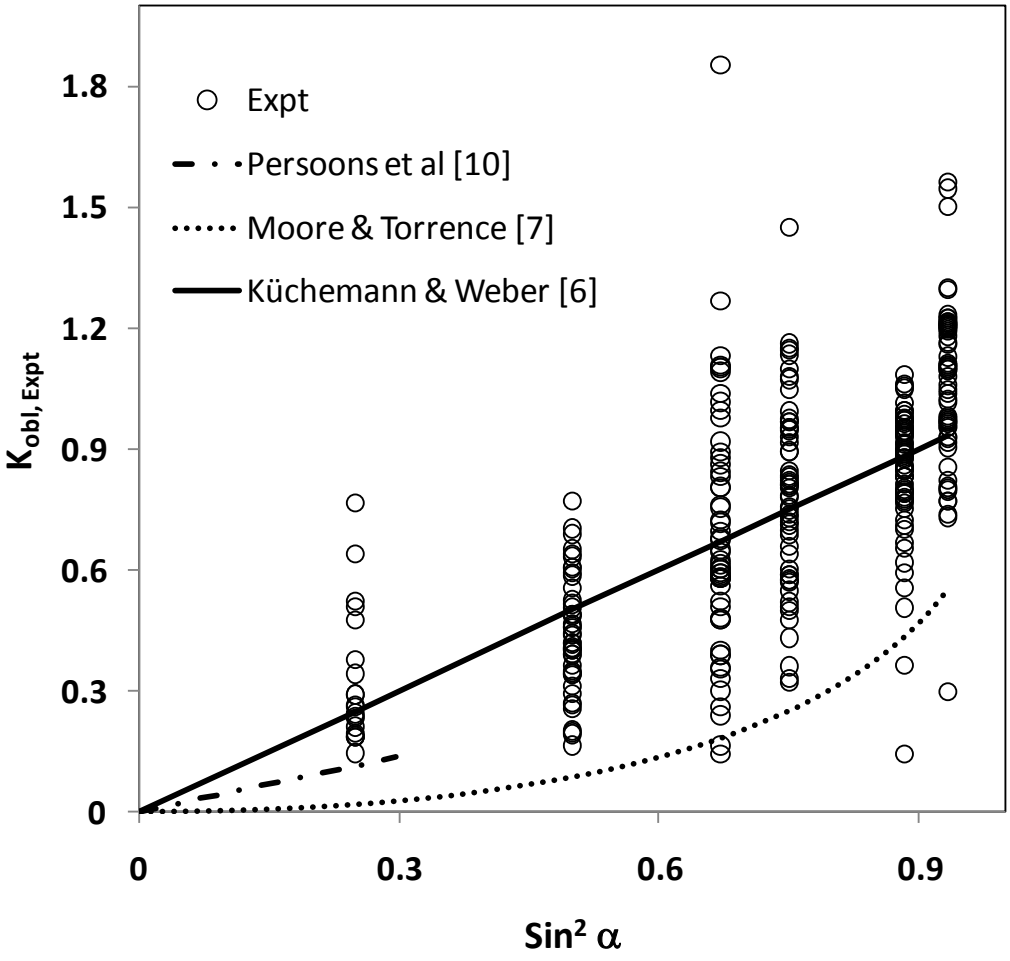

Fig 7 Comparison of K_{Obl} against the theoretical assumption of $Sin^2\alpha$

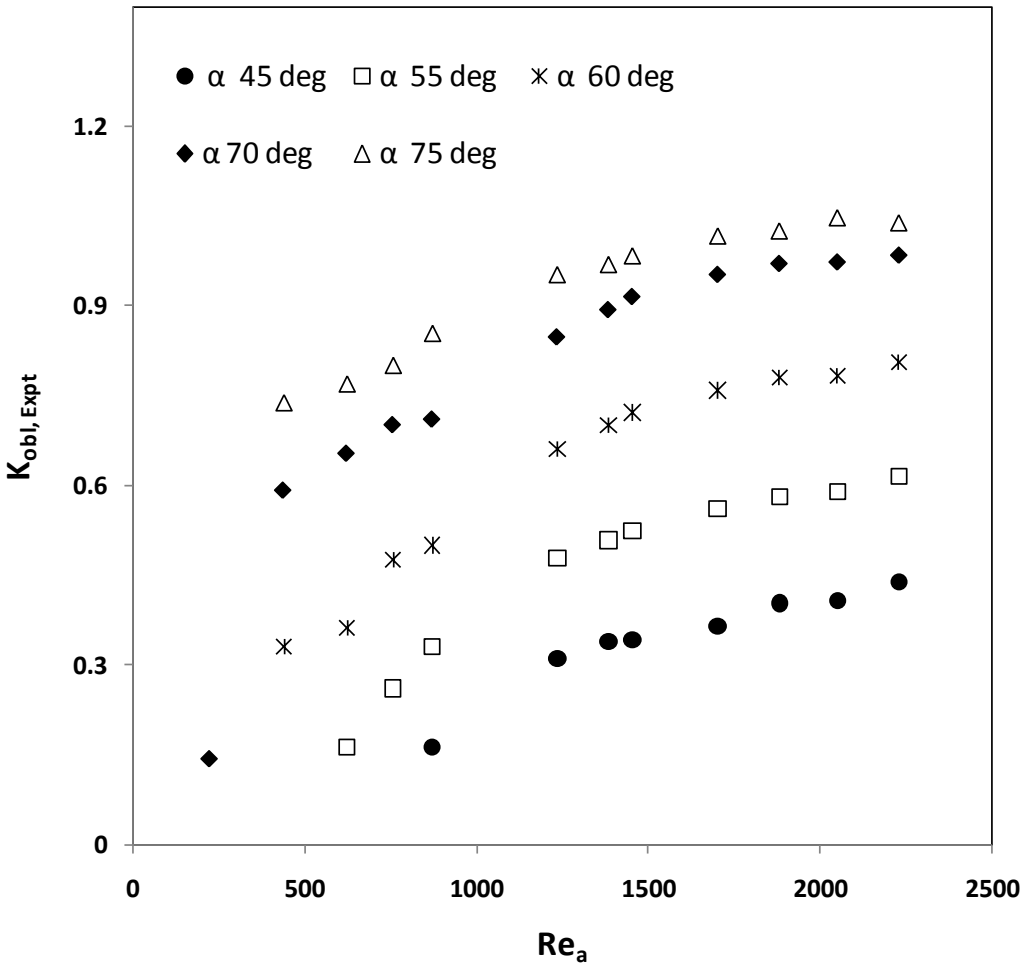

Figure 8 K_{Obl} dependence on approach Reynolds number (Re_a) for 27 mm monolith

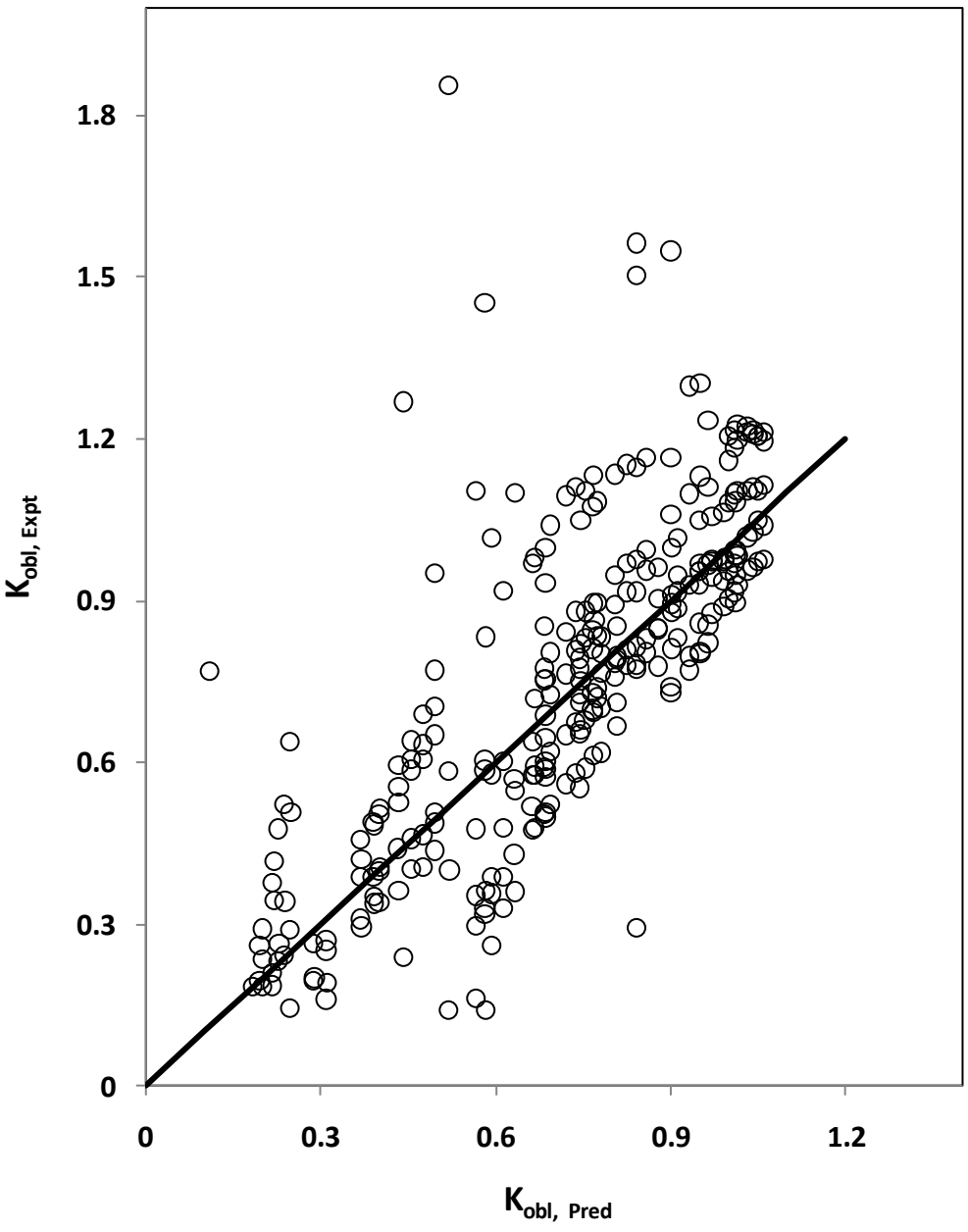

Fig 9 Comparison of experimental and predicted K_{Obl} using equation (12)

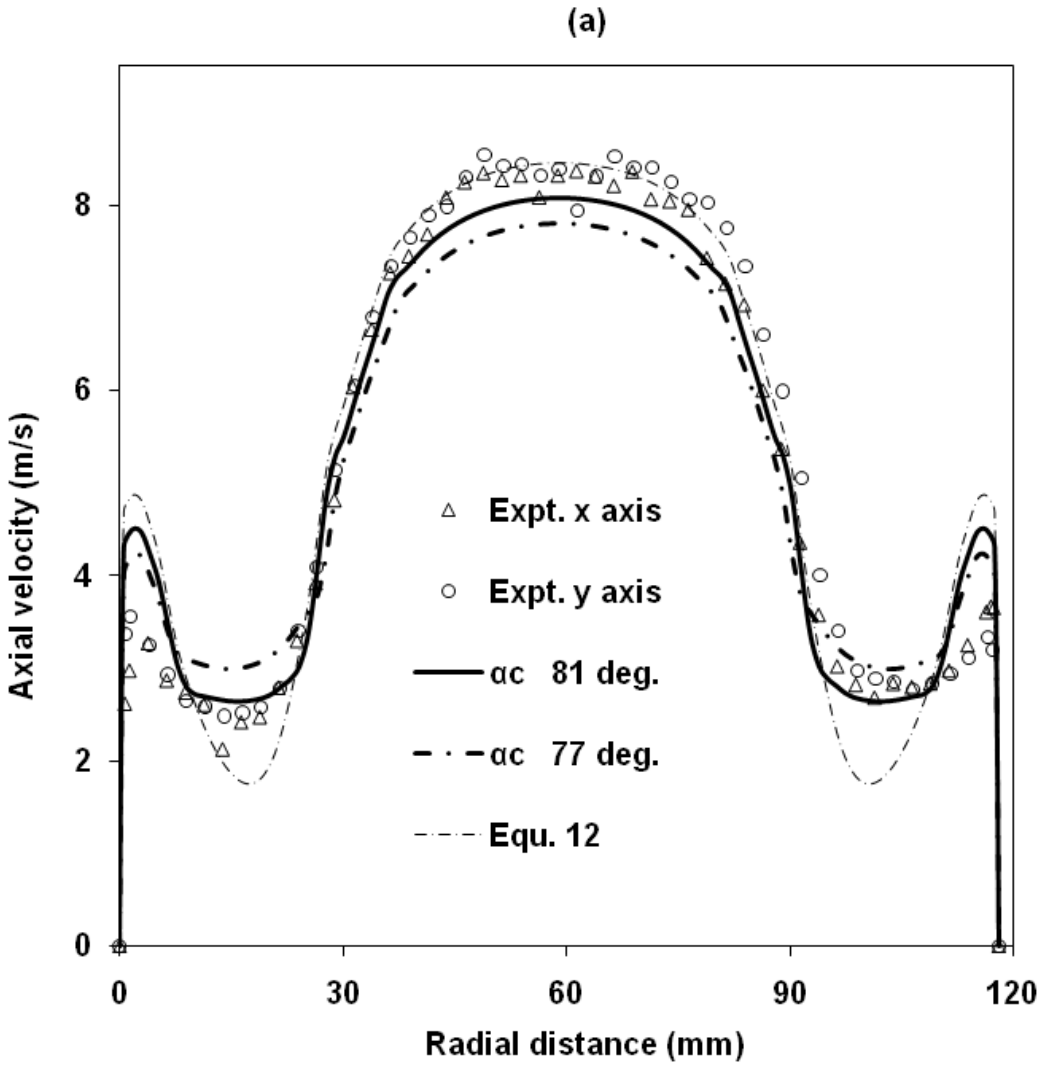
(a)
Axial velocity (m/s)
0
2
4
6
8
0
30
60
90
120
Radial distance (mm)
Expt. x axis
Expt. y axis
αc 81 deg.
αc 77 deg.
Equ. 12

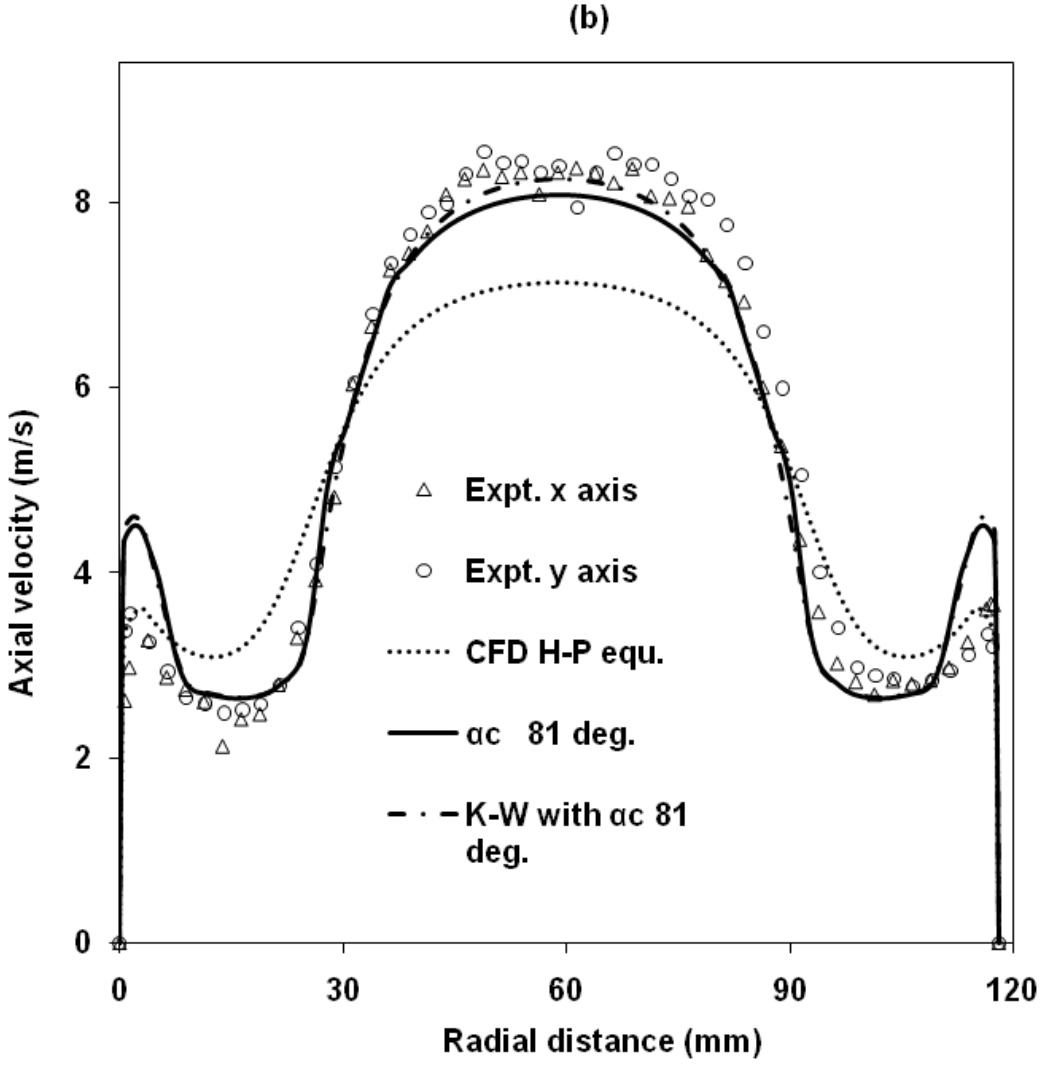
(b)
Axial velocity (m/s)
0
2
4
6
8
0
30
60
90
120
Radial distance (mm)
Expt. x axis
Expt. y axis
CFD H-P equ.
αc 81 deg.
K-W with αc 81 deg.

(c)

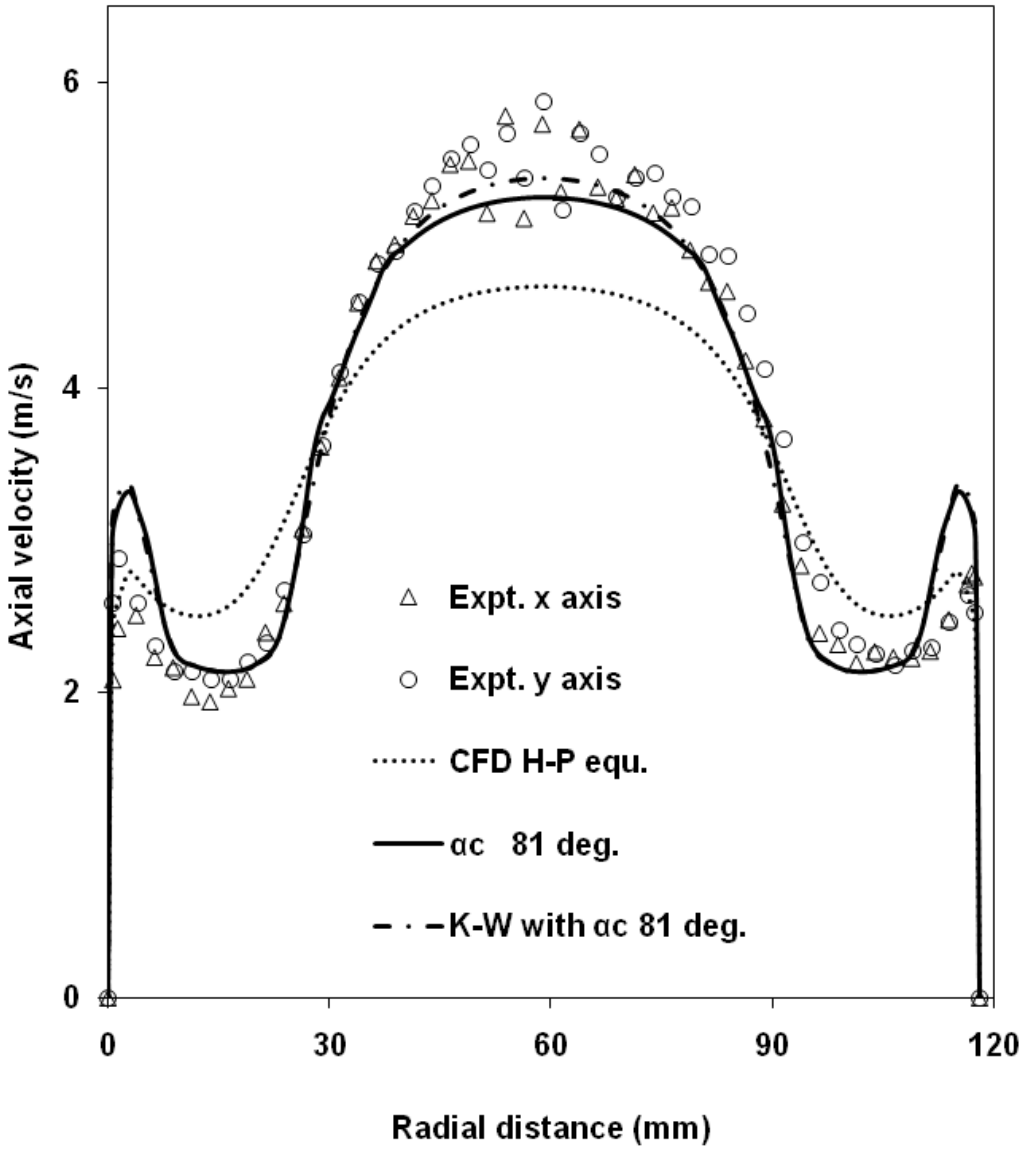
Axial velocity (m/s)
6
4
2
0
0
30
60
90
120
Radial distance (mm)
Expt. x axis
Expt. y axis
CFD H-P equ.
αc 81 deg.
K-W with αc 81 deg.

(d)

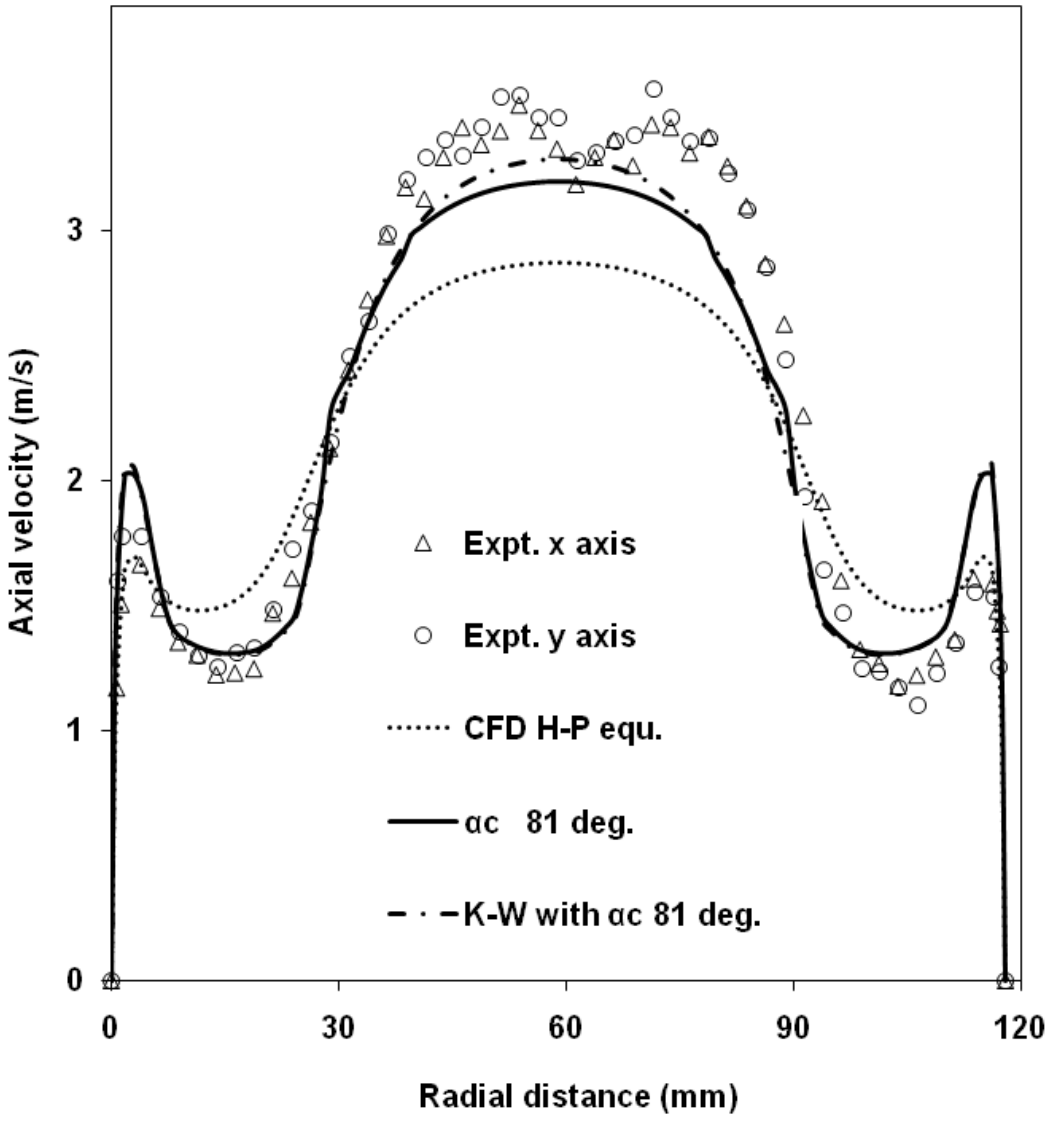
Axial velocity (m/s)
0
1
2
3
0
30
60
90
120
Radial distance (mm)
Expt. x axis
Expt. y axis
CFD H-P equ.
αc 81 deg.
K-W with αc 81 deg.

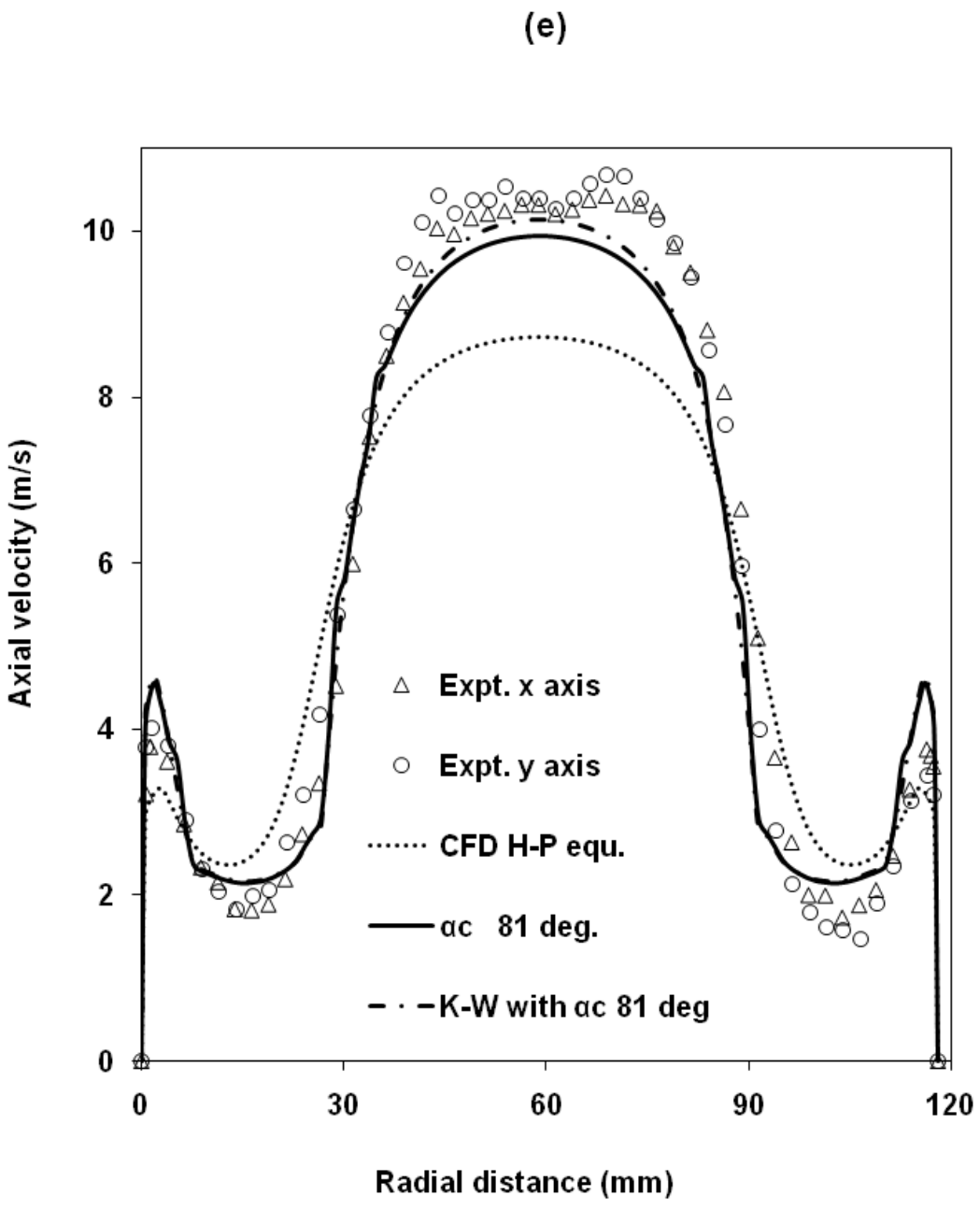

Fig 10 Comparison between experimental data (symbols) and CFD predictions (line curves). (a) 152 mm monolith; *Re* 79900. CFD: equ. (12) with/without α_c (b) 152 mm monolith; *Re* 79900. CFD: K-W and equ. (12) both with α_c and H-P (no oblique losses). (c) 152 mm monolith; *Re* 58300. CFD: as (b). (d) 102 mm monolith; *Re* 35900. CFD: as (b). (e) 102 mm monolith; *Re* 83200. CFD: as (b).

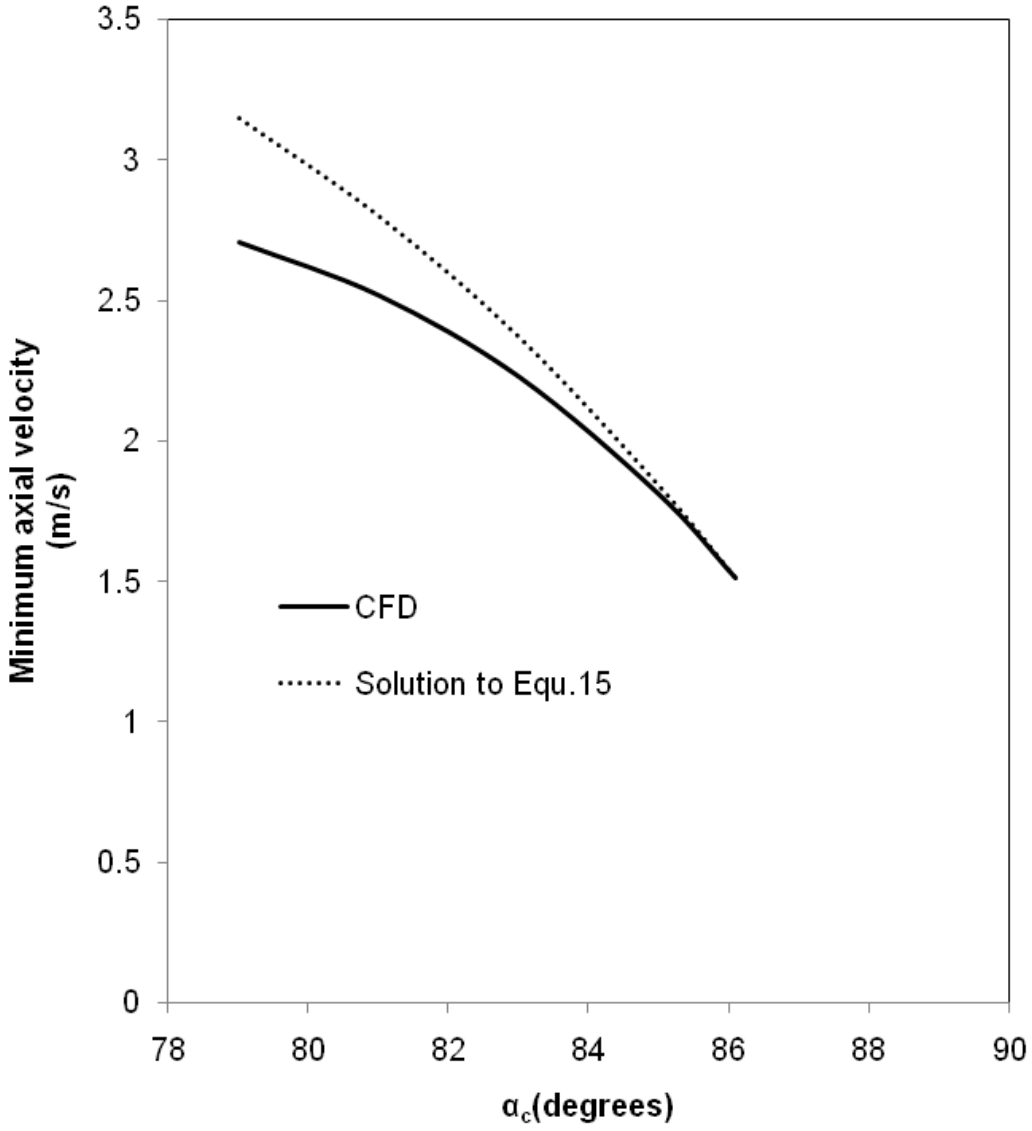

Fig 11 Minimum axial velocities immediately upstream of the 152 mm monolith at *Re* 79900